



UNIVERSITY OF LEEDS

This is a repository copy of *Modes of Interaction of Pleckstrin Homology Domains with Membranes: Toward a Computational Biochemistry of Membrane Recognition*.

White Rose Research Online URL for this paper:  
<http://eprints.whiterose.ac.uk/125266/>

Version: Accepted Version

---

**Article:**

Naughton, FN, Kalli, AC [orcid.org/0000-0001-7156-9403](http://orcid.org/0000-0001-7156-9403) and Sansom, MSP (2018) Modes of Interaction of Pleckstrin Homology Domains with Membranes: Toward a Computational Biochemistry of Membrane Recognition. *Journal of Molecular Biology*, 430 (3). pp. 372-388. ISSN 0022-2836

<https://doi.org/10.1016/j.jmb.2017.12.011>

---

© 2017 Published by Elsevier Ltd. This manuscript version is made available under the CC-BY-NC-ND 4.0 license <http://creativecommons.org/licenses/by-nc-nd/4.0/>

**Reuse**

This article is distributed under the terms of the Creative Commons Attribution-NonCommercial-NoDerivs (CC BY-NC-ND) licence. This licence only allows you to download this work and share it with others as long as you credit the authors, but you can't change the article in any way or use it commercially. More information and the full terms of the licence here: <https://creativecommons.org/licenses/>

**Takedown**

If you consider content in White Rose Research Online to be in breach of UK law, please notify us by emailing [eprints@whiterose.ac.uk](mailto:eprints@whiterose.ac.uk) including the URL of the record and the reason for the withdrawal request.



[eprints@whiterose.ac.uk](mailto:eprints@whiterose.ac.uk)  
<https://eprints.whiterose.ac.uk/>

**Modes of interaction of pleckstrin homology domains with membranes: towards a computational biochemistry of membrane recognition.**

*Fiona B. Naughton<sup>1</sup>, Antreas C. Kalli<sup>1,2</sup> & Mark S.P. Sansom<sup>1\*</sup>*

<sup>1</sup>Department of Biochemistry  
University of Oxford  
South Parks Road  
Oxford  
OX1 3QU  
U.K.

<sup>2</sup>Leeds Institute of Cancer and Pathology  
St James' University Hospital  
School of Medicine  
University of Leeds  
Leeds  
United Kingdom

\*to whom correspondence should be addressed.

Email [mark.sansom@bioch.ox.ac.uk](mailto:mark.sansom@bioch.ox.ac.uk)

Direct: +44 (0)1865-613306

PA: +44 (0)1865-613212

*J. Molec. Biol.*, ms. JMB-D-17-00453R1

**Abstract**

Pleckstrin homology (PH) domains mediate protein-membrane interactions by binding to phosphatidylinositol phosphate (PIP) molecules. The structural and energetic basis of selective PH-PIP interactions is central to understanding many cellular processes, yet the molecular complexities of the PH-PIP interactions are largely unknown. Molecular dynamics (MD) simulations using a coarse-grained model enables estimation of free energy landscapes for the interactions of 12 different PH domains with membranes containing PIP<sub>2</sub> or PIP<sub>3</sub>, allowing us to obtain a detailed molecular energetic understanding of the complexities of the interactions of the PH domains with PIP molecules in membranes. Distinct binding modes, corresponding to different distributions of cationic residues on the PH domain, were observed, involving PIP interactions at either the ‘canonical’ (C) and/or ‘alternate’ (A) sites. PH domains can be grouped by the relative strength of their C- and A-site interactions, revealing that a higher affinity correlates with increased C-site interactions. These simulations demonstrate that simultaneous binding of multiple PIP molecules by PH domains contributes to high affinity membrane interactions, informing our understanding of membrane recognition by PH domains *in vivo*.

## INTRODUCTION

The interactions of peripheral membrane proteins with cell membranes are vital for many cellular processes, including many signalling pathways<sup>1</sup>. These interactions are mediated by lipid binding domains, such as the PH, PX, FYVE and C1 domains, which often exhibit a preference for specific membrane lipids<sup>2; 3</sup>. A common target for lipid-binding domains are the phosphoinositol phosphates (PIPs), a family of seven anionic lipids distinguished by different phosphorylation patterns of an inositol head-group<sup>4; 5; 6</sup>. They are present in membranes throughout the cell in varying concentrations and may be interconverted in response to signalling events<sup>2; 4; 5; 6</sup>. PI(4,5)P<sub>2</sub>, for example, is constitutively present in the inner leaflet of the plasma membrane, and may be phosphorylated to produce PI(3,4,5)P<sub>3</sub>, which acts as a second messenger in pathways related to cell survival and metabolism<sup>7</sup>.

Pleckstrin homology (PH) domains are among the most common membrane binding domains and are known to bind PIPs<sup>2; 8</sup>. Despite sharing a common fold, sequence variations between PH domains allow them to bind PIPs with differing selectivities and affinities<sup>8</sup>. In this way, PH domains are able to effectively target specific membranes in both a temporal and spatial fashion<sup>3; 4; 6</sup>. Aberrant behaviour in recruitment of peripheral proteins to membranes, including those involving PH domains, is in many cases associated with disease<sup>9</sup>; for example, the PH domains of BTK and AKT1 have been associated with X-linked agammaglobulinemia<sup>10</sup> and cancer<sup>11</sup>, respectively. Understanding the molecular details, both structural and energetic, of PH domain-PIP interactions, and indeed of protein-membrane interactions (PMIs) in general, is therefore of interest, especially in the context of the potential druggability of PMIs of peripheral membrane proteins<sup>12; 13</sup>.

A number of experimental techniques are available for the study of lipid-protein interactions<sup>14</sup>, many of which have been applied to PH domains. Structures determined for PH domains bound to PIP analogues (generally inositol phosphates, i.e. the headgroups of the corresponding PIP lipid molecules, see e.g.<sup>15; 16; 17; 18; 19; 20; 21; 22; 23; 24</sup>) suggest the presence of two possible PIP-interactions sites: the 'canonical' or C-site, and a less common 'alternate' or 'atypical'/A-site<sup>3</sup> (Figure 1A). These sites have also been confirmed through e.g. mutational<sup>16; 23; 25; 26; 27; 28</sup> and NMR<sup>16; 29; 30; 31</sup> studies.

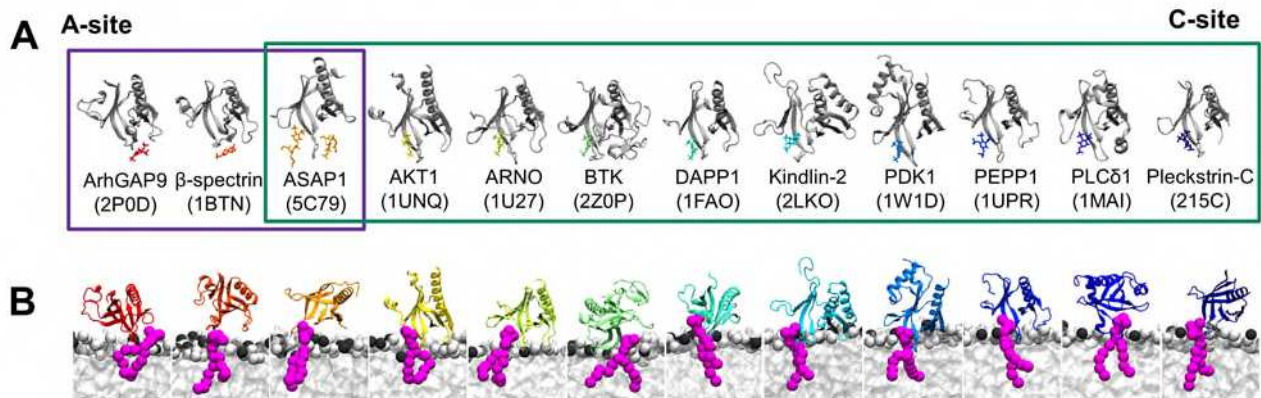


**Figure 1 – A.** Structures of PH domains with bound PIP analogues as seen in the PDB. Each domain has been aligned to the same reference structure. PIP analogues may be bound in the canonical (C-site) and/or alternate (A-site) sites, as indicated. **B.** Structures from molecular dynamics simulations showing representative binding modes, occurring at the minima of the calculated free energy profiles, for each domain interacting with a PIP-containing membrane.

Affinities of PH domains for PIP lipids have been quantified using a number of biophysical techniques including isothermal titration calorimetry (ITC) and surface plasmon resonance (SPR). Together with more qualitative methods for assessing lipid selectivity, such studies have reported PH domains to be selective for PIP<sub>2</sub>, PIP<sub>3</sub>, or other PIPs, with affinities ranging from low nanomolar to micromolar or above (Supplementary Table S3). These studies, however, have often employed water soluble PIP analogues<sup>14</sup>, a simplification of PIP molecules and the native membrane environment in which PH domains function. The properties estimated, including dissociation constants, vary between experiments: for example affinities of the AKT1-PH domain for PIP<sub>3</sub> or its analogues vary from 0.023  $\mu$ M (using FRET<sup>32</sup>) to 1.5  $\mu$ M (using a fluorescence assay<sup>33</sup>). This degree of variation can make it difficult to understand how the structural basis of molecular recognition at the protein-membrane interface of diverse PH domains in turn determines how PH domains localize to different classes of membrane within a cell.

Molecular dynamics (MD) simulations can be used to investigate PMIs at atomistic or near-atomistic detail, and have been demonstrated to agree with and to complement experimental studies<sup>34; 35</sup>. They have been used to explore the PMIs of e.g. PH domains<sup>36; 37; 38; 39; 40; 41; 42; 43; 44</sup>, and of C2 domains<sup>45; 46; 47</sup>. One may use MD simulations to estimate binding free energies for protein/ligand interactions<sup>48</sup>. For example, Umbrella Sampling (US)<sup>48</sup> may be used to obtain a one-dimensional free energy profile (often referred to as a potential of mean force, PMF) profile along a particular ‘reaction coordinate’ such as a protein-lipid separation distance. The use of a ‘physical’ reaction coordinate allows additional structural insights to be made. PMF calculations can be combined with coarse-grained (CG) MD simulations (in which groups of around four heavy atoms

are represented by a single particle<sup>49</sup>) to describe the free energy landscapes for the interaction of lipids with integral membrane proteins, including e.g. cytochrome c oxidase<sup>50</sup> and the ADP/ATP transporter<sup>51</sup>. There also has been discussion of how to determine the convergence of such calculations<sup>52</sup>. Building upon these methods, we recently demonstrated that this approach used to describe the binding of the canonical GRP1-PH domain to a model membrane containing PIP molecules<sup>39</sup>. The results of these computational studies were consistent with the known structures of GRP1-PH interacting with PIP analogues, and with experimental selectivity and mutational data, thus demonstrating the value of CG PMF calculations for exploring PH domain PMIs in a quantitative fashion.

In a previous study<sup>42</sup> we showed that CG MD simulations could reproduce the PIP binding structures of 13 different PH domains, and predict binding orientations of these domains to PIP-containing membranes. These simulations also allowed us to confirm and refine the two sites (C-site and A-site) for PIP<sub>2</sub> on the ASAP1 PH domain<sup>23</sup>. However, we wish to determine whether we can use MD more broadly to extend beyond structural data and use simulations and PMF calculations to move towards a ‘computational biochemistry’ of PH/membrane interactions, i.e. to predict structures, strengths and specificities of PMIs to characterise the range of membrane recognition/binding modes across the family of PH domains. Thus, in the current study, we employ our previous methodology to examine the PMIs of 12 PH domains with model membranes containing PI(4,5)P<sub>2</sub> or PI(3,4,5)P<sub>3</sub> lipids (Figure 1). This enables a systematic comparison of the strength, and specificity of PIP interactions within this family of lipid-binding domains, and provides a comparative, global definition of the different modes of binding of PH domains to PIP-containing bilayers. More generally, it demonstrates the feasibility of using ‘computational biochemistry’ to characterise the interactions of peripheral proteins with their target membranes.

## RESULTS & DISCUSSION

### *Overview of the approach adopted*

It is useful to consider the overall approach we have adopted to analysing the interactions of PH domains with PIP-containing membranes. The PH domains selected for simulation were those for which structures bound to PIP (or IP) analogues are available (Figure 1; 12 structures in total) in the Protein Data Bank. Umbrella Sampling (US) simulations for each domain binding to both PI(4,5)P<sub>2</sub> (i.e. PIP<sub>2</sub>) and PI(3,4,5)P<sub>3</sub> (i.e. PIP<sub>3</sub>) were set up and performed as outlined in Figure 2 in order to estimate PMFs, i.e. one dimensional free energy profiles for the interaction of each PH domain with PIP-containing lipids bilayers. Each crystal structure was aligned relative to a preassembled bilayer by superimposing the headgroup of the PIP lipid with the corresponding bound PIP analogue,

before conversion to a coarse-grained representation (Figure 2). For ASAP1, where the crystal structure contains two bound PIP analogues, two structures were generated by aligning to each bound ligand in turn. The bilayer contained both zwitterionic (phosphatidylcholine, PC) and anionic (phosphatidylserine, PS) lipids in a 80:20 ratio in order to mimic the overall electrostatic environment presented by a mammalian cell membrane, in addition to one PIP molecule to which the PH domain was bound.

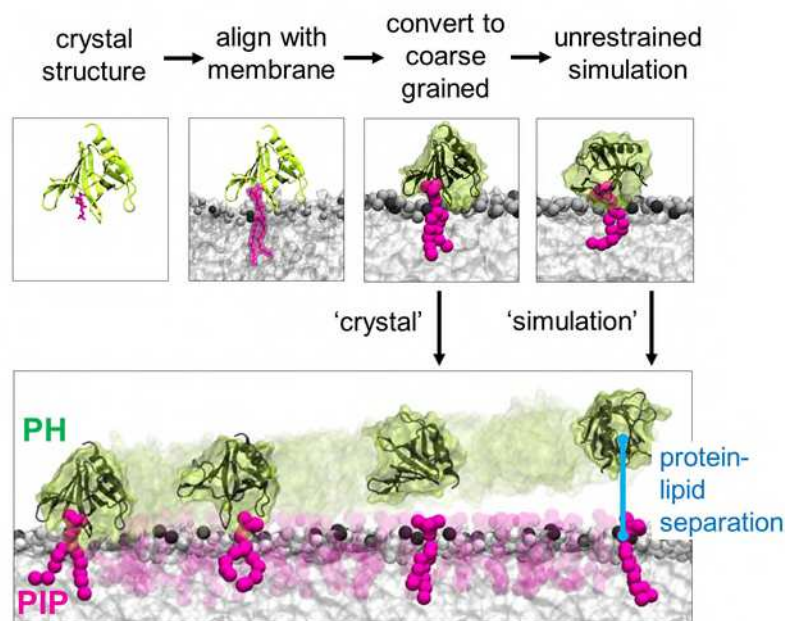


**Figure 2** – Overview of the simulation process, shown for the PH domain of ARNO (yellow) binding to PIP<sub>3</sub> (magenta). The panel below shows snapshots taken from the umbrella sampling simulation windows; the ‘protein-lipid separation’ reaction coordinate used is indicated by the blue line linking the two centres of mass. The protein is shown with a cartoon representation when an atomistic resolution is used, and as a surface representation (with cartoon of the crystal structure in black for reference) where coarse-grained. The bilayer is shown with a surface representation, with POPC and POPS phosphates shown explicitly in light and dark grey, respectively. Water molecules are present in the simulation but have been omitted from this and other figures for clarity.

The above aligned structure was used as the ‘crystal’ initial structure for umbrella sampling (US). The reaction coordinate was chosen to be protein-lipid separation along the membrane normal, measured from protein centre-of-mass to the PIP 1’ phosphate (see Figure 2). Calculation of PMFs is critically dependent on the way in which the initial configurations have been obtained. Accordingly, to assess the robustness/sensitivity of the results to the exact starting model, a parallel set of US simulations were performed using in each case a slightly different initial structure (‘simulation’) obtained from an unrestrained 1  $\mu$ s CG simulation starting from the ‘crystal’ configuration (see Methods for details). In these ‘simulation’ configurations, the PH/PIP

interactions were optimised and in some cases, they differed from the PH/PIP complex crystal/NMR structures (Supplementary Figure S6). This demonstrates that when using rather different starting structures this methodology yields similar PMF profiles, which provides a degree of confidence that the PMF estimates are robust to this aspect of their calculation. In principle one might further evaluate the robustness of PMFs by reversing the reaction coordinate (i.e. by starting with an unbound PH domain; see e.g. <sup>52</sup> for a discussion of the application of this to lipid/integral membrane protein interactions). However, in the current study we are evaluating the more complex interaction of a protein (the ‘ligand’) with a dynamic PIP-containing bilayer surface (the ‘receptor’) which makes this apparently simple approach rather problematic to implement.

### *Free energy profiles*

Analysis of free energy profiles allows us to compare strengths of interactions with PIP-containing membranes between the different PH domains, and between simulations and experiments. Each of the 1D potentials of mean force (PMFs) showed a clear global minimum corresponding to a tightly bound state, ‘T’, at a protein-lipid separation of ca. 1.5 nm for most systems, or around 2.2 nm in some cases for e.g.  $\beta$ -spectrin and BTK (see Figure 3 for the PIP<sub>2</sub> PMFs and Supplementary Figure S1 for the PIP<sub>3</sub> PMFs). Many profiles also show a local minimum or inflection at this distance, corresponding to a more loosely bound state ‘L’ (indicated for ArhGAP9 in Figure 3). The well depths for the T state (i.e. the global minimum) ranged from ca. -40 (PDK1) to -10 kJ/mol (ASAP1). Overall, the PMFs were in good agreement between the two different starting structures for each protein-lipid system, with the exception of BTK.

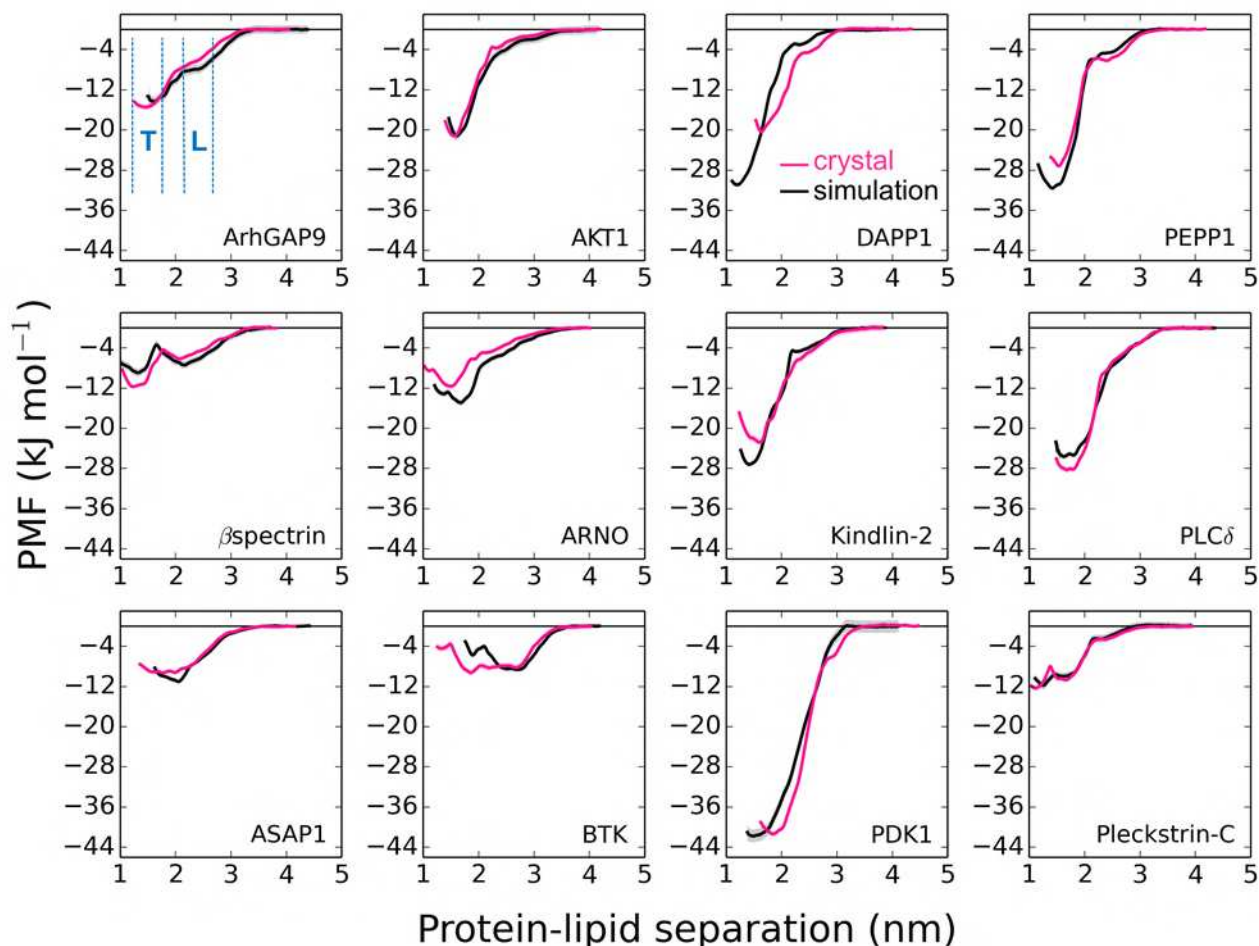


**Figure 3** – Potentials of Mean Force (PMFs) calculated for each of the studied PH domains binding to PIP<sub>2</sub>, using initial structures from directly aligning the crystal structure (magenta) or taken following simulation (black). Bootstrap errors are shown. The ‘tightly’ (T) and ‘loosely’ (L) bound regions – defined for each system relative to the profile minimum – are indicated for ArhGAP9 in the first panel. ASAP1 profiles are shown for the initial structure aligned by the C-site PIP molecule. Note that bootstrap error estimation does not take into account errors due to incomplete sampling and so it is likely that this underestimates the ‘total’ error.

Comparing the energy minima (i.e. well depths) across all the protein/lipid systems demonstrates good agreement between profiles obtained from the ‘crystal’ and ‘simulation’ structures, with only BTK (binding to PIP<sub>3</sub>) and DAPP1 (binding to both PIP<sub>2</sub> or PIP<sub>3</sub>) showing variation greater than a ‘chemical accuracy’ of ~4 kJ/mol (Figure 4A). The PMFs may be used to obtain standard free energies of binding for each PH-PIP system (see<sup>53</sup> for the basis of the method for accounting for the effects of restraints and for use of a one dimensional PMF in this calculation). These values are shown in Figure 4C, along with values derived from reported experimental dissociation constants (see also Supplementary Table S3). A previous study<sup>54</sup> predicting possible membrane interaction sites across PH domains, including those studied here, failed to identify any sites for ArhGAP9, β-spectrin or BTK, in line with the lower binding energies of these domains seen here.

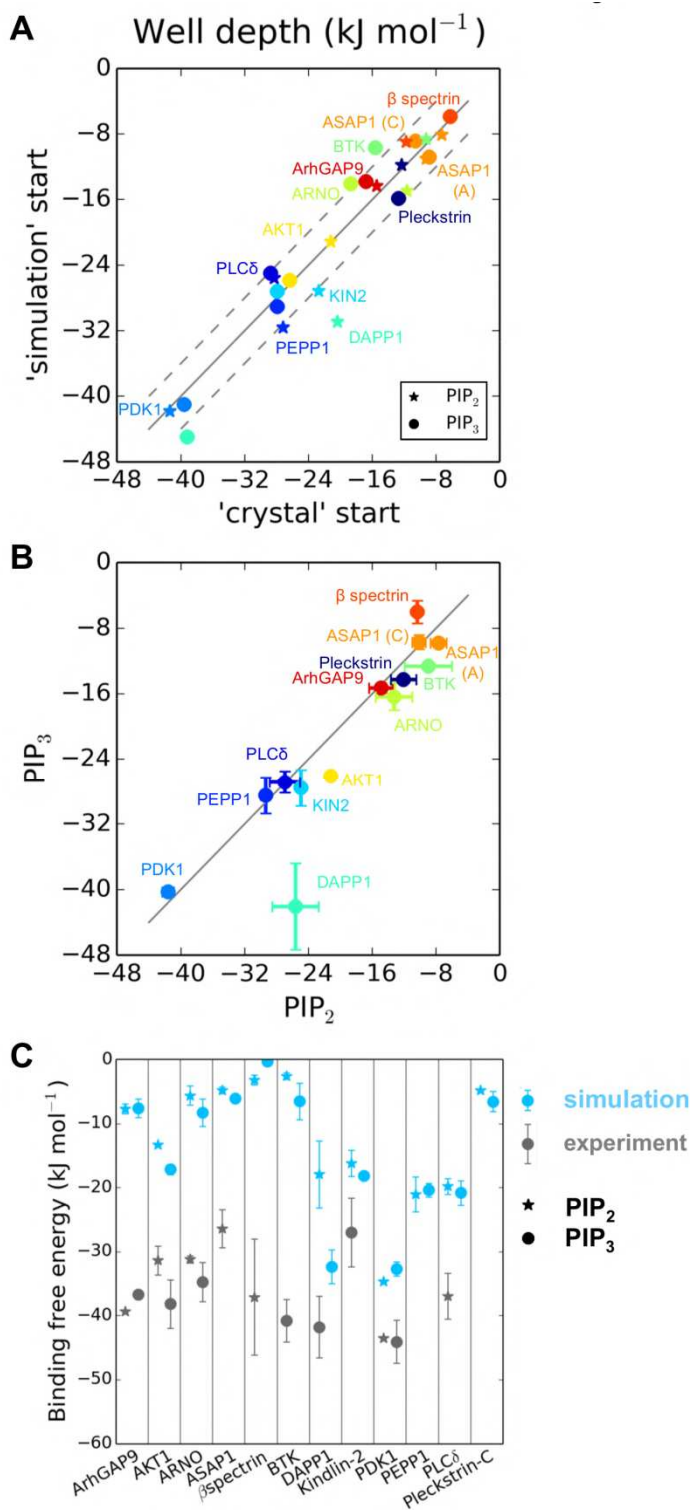


**Figure 4.** **A.** Well depths from the free energy profiles calculated from the ‘crystal’ start vs. ‘simulation’ start for each PH-PIP system. The dotted lines indicate a difference of 4 kJ/mol. **B.** Average well depths of profiles calculated for each PH domain binding to PIP<sub>3</sub> vs PIP<sub>2</sub>, indicating selectivity (domains falling above the dotted line indicates preference for PIP<sub>2</sub>; below the line for PIP<sub>3</sub>). Error bars indicate the range from the two US simulations. **C.** Comparison of PH-PIP binding free energies as obtained in this study (blue) and average of experimental results (grey; see Supplementary Table S3). Errors indicate standard deviation.

The binding free energies derived from the simulations are in general smaller than those measured experimentally (see Figure 4C for an overall comparison). This may be in part due to limitations in the coarse-grained model used, although if anything the CG forcefield might be anticipated to overestimate the strength binding to a lipid bilayer. There are also some variations within and between the experimental data (obtained by a range of different methods; Supplementary Table S3) such that  $K_D$  values for a given PH-PIP (or PIP analogue) interaction often vary over several orders of magnitude. AKT1-PH, for example, has been reported to bind to PIP<sub>3</sub> with a  $K_D$  of 0.023  $\mu$ M (using FRET<sup>32</sup>) and of 0.59  $\mu$ M (using SPR<sup>55</sup>), and to IP<sub>4</sub> (the headgroup of PIP<sub>3</sub>) with a  $K_D$  of 1.5  $\mu$ M (using a fluorescence based assay<sup>33</sup>). Many studies employ either PIPs or their water soluble analogues either spotted onto a surface or in solution, neither of which fully reflects the membrane environment in which PIP-binding occurs *in vivo*. Furthermore, even in a membrane context, dependence of PH-PIP interactions on experimental conditions including pH<sup>56</sup>, salt concentration<sup>57</sup>, buffer<sup>58</sup> and lipid composition<sup>56; 57; 59; 60; 61</sup> has been demonstrated. This makes it difficult to compare directly results obtained from different studies, both experimental and computational.

Having said this, it is difficult to suggest that such variations explain the overall difference between  $K_D$ s in the 0.1  $\mu$ M range (i.e.  $\Delta G$  ca. -40 kJ mol<sup>-1</sup>) from experimental studies and those in the 0.1 mM range (i.e.  $\Delta G$  ca. -20 kJ mol<sup>-1</sup>) derived from the PMFs. A more likely explanation lies in the *number* of PIP molecules interacting when a PH domain binds to a PIP-containing membrane or equivalent surface. In particular, only one PIP molecule was present in the current PMF calculations. Previous computational studies<sup>41; 42; 43; 62</sup> have suggested that binding of a PH domain may result in local nanoscale clustering of PIP molecules, and thus a single PH domain may interact with multiple PIP molecules at the same time. Similar effects have been suggested by a number of experiments. For example, in a recent study of the kindlin 3 PH domain, Ni et al.<sup>40</sup> demonstrated by SPR that when PIP<sub>3</sub> was immobilized (which would be expected to measure each PH molecule binding to a single PIP molecule) the  $K_D$  was 0.3 mM, whereas when the PH domain was immobilized and binding to PIPs in a lipid nanodisc (which would enable multiple PIP molecules to interact with a single PH domain), a 3 orders of magnitude lower  $K_D$  (0.4  $\mu$ M) was obtained. Thus, it should be emphasized that the binding free energies estimated in the current study correspond to 1:1 PH-PIP interactions, at the surface of a lipid bilayer.

The PIP selectivity<sup>63; 64</sup> of each PH domain observed in the simulations may also be assessed by comparing the well depths from the PIP<sub>3</sub> and PIP<sub>2</sub> PMF profiles (Figure 4B). Most PH domains bound equally strongly to PIP<sub>3</sub> and PIP<sub>2</sub>, at least at the current CG level of description. Only the AKT1, DAPP1 and  $\beta$ -spectrin PH domains were predicted to exhibit clear-cut selectivity: AKT1 showed 4.5-fold selectivity for PIP<sub>3</sub>; DAPP1 showed 300-fold selectivity for PIP<sub>3</sub>; whilst  $\beta$ -spectrin

showed 3-fold selectivity for PIP<sub>2</sub>. Direct comparison with experiment is again hindered by the lack of *quantitative* data. However, these three domains are generally reported to have the same PIP<sub>2</sub> vs. PIP<sub>3</sub> selectivity as predicted computationally (see Supplementary Figure S5). In the case of DAPP1, simulation suggests 300-fold selectivity for PIP<sub>3</sub> compared to >250-fold from experiment. Three additional domains are suggested from experiment to be PIP<sub>3</sub>-selective (ARNO, BTK and kindlin-2). For these the computational results suggest a small degree of PIP<sub>3</sub> selectivity. Inconsistency between computational and experimental results is seen for the PH domain of PLCδ1, which in most (but not all) cases is observed experimentally to be PIP<sub>2</sub> selective, while non-selective computationally.

#### *Effect of mutations on PH/PIP association*

A test of the biological significance of free energy profiles is possible by comparison of a wild type and a mutant PH domain. To further examine the sensitivity of PMFs to the details of PH domain structure, and the degree of agreement of the calculated PMFs with available experimental data, one may explore the effect of mutations to PH domains on interactions with PIPs. For example, the oncogenic E17K mutation in the AKT1 PH domain has been characterised both *in vitro* and *in vivo*<sup>32</sup>. This mutation is found in patients with breast and colorectal cancers, and results in a substantive increase in the affinity of the AKT1 PH domain for PIP<sub>2</sub> and for PIP<sub>3</sub>. We have calculated the PMFs for PIP<sub>2</sub> (and PIP<sub>3</sub>) of the E17K mutant and compared with those of the wildtype AKT1 PH domain (see Figure 5). The results of these calculations suggest that the mutation does indeed result in a ca. -20 kJ mol<sup>-1</sup> decrease in the free energy of binding of the AKT1 PH domain to PIP<sub>2</sub> and PIP<sub>3</sub>. Simulations in which the PIP was initially bound to the C-site of the ArhGAP9 PH domain resulted in similar PMF profiles to the simulations when the PIP was initially bound to the A-site of the ArhGAP9 PH. This demonstrates that the PH domains in our simulations can explore a range of different orientations (Supplementary Figure S8).

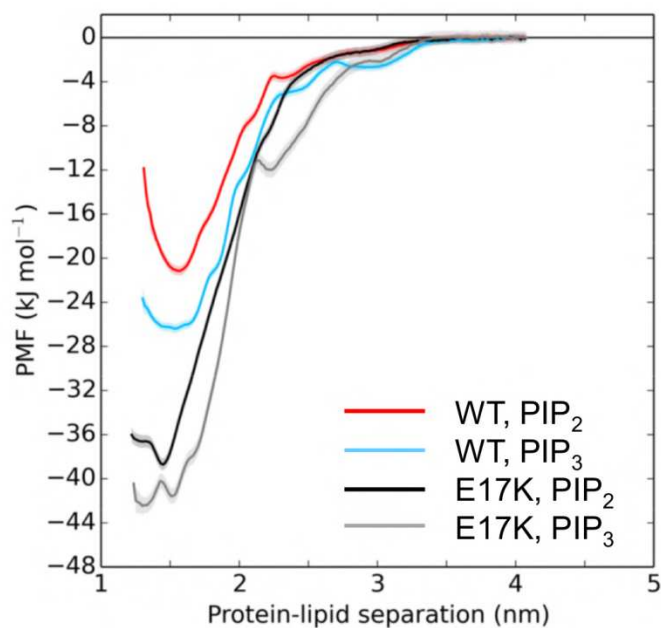


**Figure 5.** PMF profiles for wild-type ATK1 (from the ‘crystal’ starting structure) and E17K mutant AKT1 binding PIP<sub>2</sub> (red and black, respectively) or PIP<sub>3</sub> (blue and grey, respectively).

To further investigate the basis of the observed selectivity and affinities, we next examine the molecular details of the PH-PIP interactions.

#### *PIP binding at the atypical and canonical sites*

Free energy landscapes reveal multiple binding sites on PH domains. This is in good agreement with a number of studies<sup>16;23;24;27</sup> that have suggested the presence of an alternate (A) PIP-binding site on PH domains, alongside and in addition to the canonical (C) site interaction. To explore in more detail the presence of multiple PIP-interaction sites on a PH domain, we defined an angle made by the PIP headgroup relative to the PH domain. This provides a simple metric to distinguish between binding at the C- and A-sites. We also estimated the relative fraction of PIP-protein contacts made with residues in the A- or the C- sites (Figure 6). A- and C- site residues were defined as equivalent residues to those known from crystal structures to contact PIP bound in the A-, or C-, site, based on a structure-based sequence alignment of the PH domains (Supplementary Figure S2), and the relative fraction of A vs. C contacts was calculated as the average fraction of the ‘A-site residues’ in contact with PIP minus the fraction of the ‘C-site residues’ in contact with PIP over each simulation frame.

Two-dimensional interaction energy landscapes were obtained by projecting the one-dimensional PMF profiles along the PIP-binding angle coordinate (Supplementary Figure S4). These landscapes revealed multiple binding sites, which are observed to different extents for different PH-PIP systems and as the protein-lipid separation is increased. Good agreement between the ‘crystal’ and

'simulation' derived landscapes is again observed. To allow comparison between PH domains, 'tightly' and 'loosely' bound regions were defined covering protein-lipid separation ranges from - 0.1 to 0.4 nm and 0.8 to 1.2 nm relative to the well minimum respectively (as indicated for ArhGAP9 in Figure 3). These regions were chosen to optimally encompass in turn the close-separation well observed in all PMFs, and the secondary feature (e.g. a well, or plateau) observed in many profiles, including that of ArhGAP9. The minimum was taken as the lowest well common to both profiles from the two starting ('crystal' and 'simulation') structures. Average distribution of PIP-binding angles and of relative A/C contacts, weighted to account for umbrella sampling restraints, were then calculated for these two regions for each PH-PIP system (Figure 6).

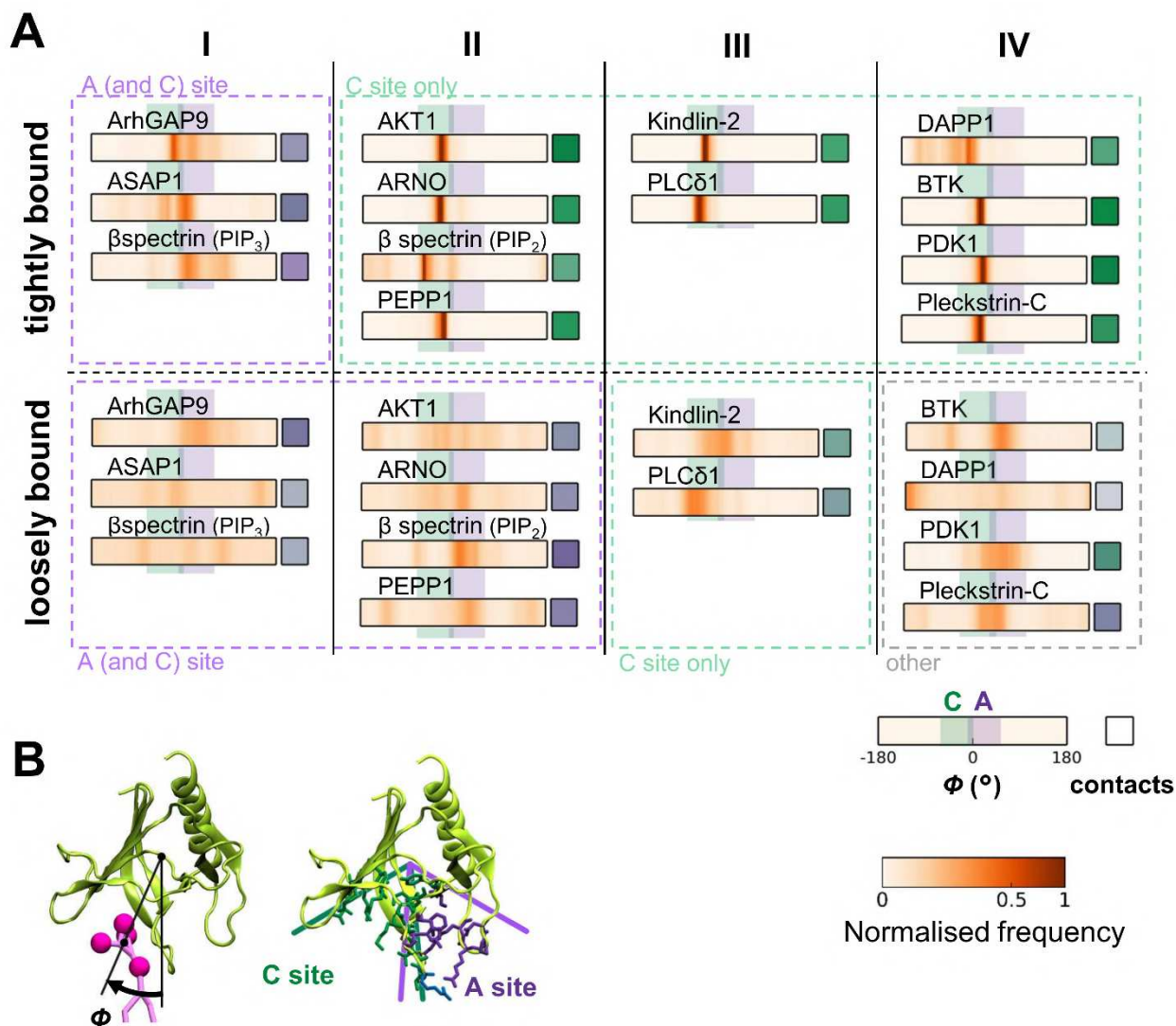


**Figure 6 A.** Distribution of PIP-binding angle and fraction of contacts with A-site (purple) or C-site (green) residues for each PH domain when in the ‘tightly bound’ or ‘loosely bound’ regions, shown for PIP<sub>2</sub> (and representative of PIP<sub>3</sub>) unless otherwise indicated. Domains are grouped by favourable binding site(s) in each region. Four groups showing different interaction patterns between the two regions are indicated. **B** The measurement of binding angle and the A-site (purple) and C-site (green) residues shown for the ARNO PH domain.

These analyses allowed us to identify preferred PIP-interaction site(s) for each PH domain when either tightly or loosely bound. This in turn revealed four main groups (Figure 6):

- **Group I:** PH domains which may bind PIP at the A-site at any separation, i.e. ASAP1, ArhGAP9, and  $\beta$ -spectrin (the latter when binding to PIP<sub>3</sub>);
- **Group II:** PH domains for which A-site interactions are observed only at larger separations, i.e. ARNO, AKT1, PEPP1, and  $\beta$ -spectrin (the latter when binding to PIP<sub>2</sub>);
- **Group III:** PH domains for which C-site interactions are favourable at both short and larger separations, and which exhibit few A-site interactions, i.e. kindlin-2, PLC $\delta$ 1; and

- **Group IV:** PH domains for which other (i.e. non-A/C- site) interactions become predominant at larger separation, i.e. BTK, DAPP1, PDK1 and pleckstrin-C.

Those PH domains which exhibit predominately C-site interactions while tightly bound (i.e. groups II, III and IV) possess the K-X<sub>n</sub>-(K/R)-X-R motif in the  $\beta$ 1 and  $\beta$ 2 strands identified previously as a requirement for PIP binding<sup>65</sup>, with additional C-site residues found on the  $\beta$ 1- $\beta$ 2,  $\beta$ 3- $\beta$ 4 and  $\beta$ 6- $\beta$ 7 loops (see Supplementary Figure S2). A-site interactions appear to require the presence of a (K/R)-X-W motif also located on the  $\beta$ 1- $\beta$ 2 loop, positioned so the sidechains face the opposite direction to those in the C-site motif, and also a long  $\beta$ 5- $\beta$ 6 loop containing a number of positively charged residues (or, in the case of ASAP1, these may be present in the  $\beta$ 6- $\beta$ 7 loop). We note, however, that some of the PH domains that exhibit predominantly C-site interactions also have a (K/R)-X-W motif or the same motif but with the W replaced by other aromatic ring sidechains. This might explain why some PH domain can bind PIPs in both A and C sites. However, it complicates the discrimination between PH domains without structural information to reveal the orientation of the sidechains in the PIP binding site.

Favourable A-site interactions while tightly bound (i.e. as seen in Group I, i.e. ArhGAP9, ASAP1 and  $\beta$ -spectrin bound to PIP<sub>3</sub>) occur when these A-site features are present but the C-site motif is absent (see Supplementary Figure S2). The presence of both sequence features (as in Group II, i.e. AKT1, ARNO and PEPP1) enables favourable PIP interactions at both sites, though the lack of A-site interactions when tightly bound suggests the C-site, when present, is generally the more favourable. DAPP1 also contains both motifs and so would be expected to be part of Group II. However, a unique ‘upside down’ orientation is seen when this domain is loosely bound, leading to its Group IV classification. This alternate orientation involves PIP interactions with the end of the PH domain helix, which has previously been predicted as a potential membrane interactions site<sup>54</sup>, but may not represent a physiological binding mode when considering the full length parent protein.

Domains which lack the A-site features (Group III and IV) may be distinguished by more positively charged or polar residues in the  $\beta$ 3- $\beta$ 4 loop of the former (PLC $\delta$ 1 and kindlin-2; Supplementary Figure S2), allowing C-site binding to be retained while loosely bound. Group IV domains instead adopt other, unique interactions, including e.g. varied ‘upside down’ orientations as for DAPP1, as described above.

#### *Modes of membrane interaction*

The interaction modes of PH domains (which may be characterised more qualitatively via unrestrained simulations of the association of PH domains with PIP-containing bilayers<sup>42</sup>) may be further distinguished by the orientation of the domain relative to the membrane. This orientation

was measured for all of the simulations and combined to provide a more ‘global’ view of PH/membrane interactions. Thus, the combined map for the ‘tightly bound’ region of the individual PMFs clearly reveals several binding modes (Figure 7). These involve PIP interacting at either the A- or C-site, with several possible orientations for each. The combined map for the ‘loosely’ bound interactions of PIPs reveal both A- and C-site binding modes, although distinct orientations relative to the bilayer normal are no longer observed. Additional ‘other’ binding modes are also seen for particular PH domains, distinct from the A/C-site interaction modes. Representative structures for the common binding modes are shown in Figure 7C and all binding modes are shown in Supplementary Figures S9 and S10.

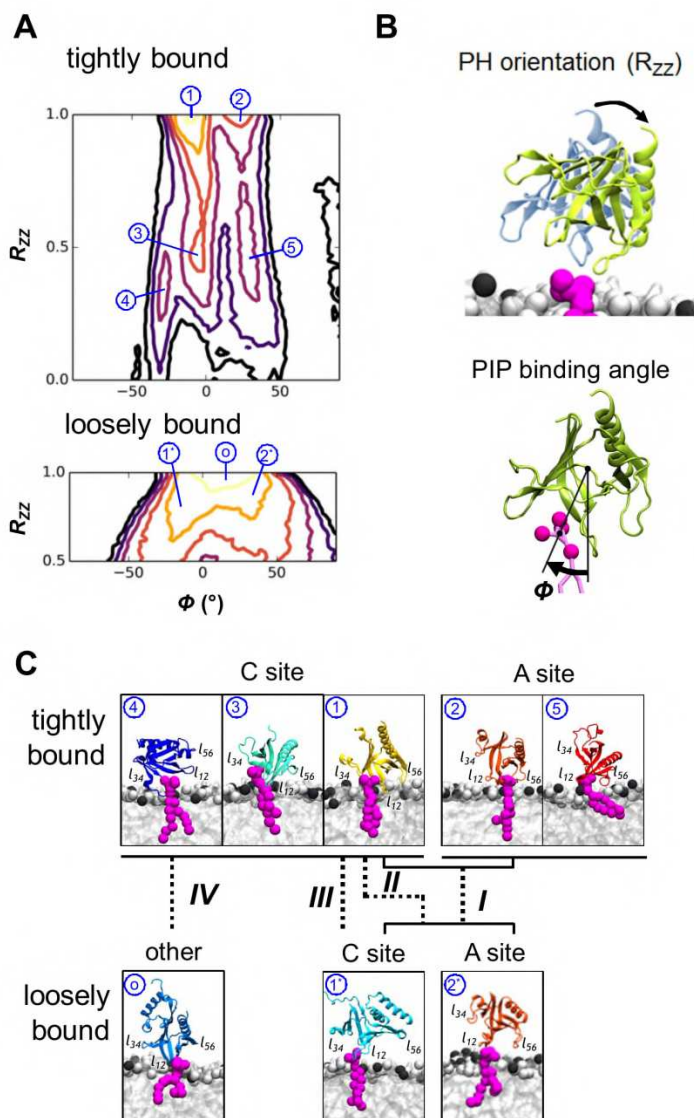


**Figure 7.** **A.** Contour map showing common binding modes in the ‘tightly’ and ‘loosely’ bound regions, based on data derived from all PH-PIP systems. Results are normalised within each group identified in Figure 6 before addition to the final combined landscape. Only a segment of the full binding landscape, containing the most frequently observed binding modes, is shown in each case. **B.** The orientation is measured as the  $R_{ZZ}$  component of the rotation matrix relative to a reference structure ( $\sim$  mode 1 in **C**). **C.** Representative structures of each of the binding modes identified in **A**. The PH domains that adopt each binding mode are as follows: while tightly bound: **1**: AKT1, ARNO, ASAP1, DAPP1, kindlin-2, PDK1, PEPP1, pleckstrin-C; **2**: ASAP1,  $\beta$ -spectrin; **3**: ArhGAP9, DAPP1, pleckstrin-C (PIP<sub>2</sub> only) and to a lesser extent AKT1; **4**:  $\beta$ -spectrin (PIP<sub>2</sub> only), BTK, PLC $\delta$ 1; **5**: ASAP1 and to a lesser extent ArhGAP9 and  $\beta$ -spectrin. While loosely bound: **0**: ASAP1, PDK1, pleckstrin; **1\***: AKT1,  $\beta$ -spectrin, kindlin-2, PEPP1, PLC $\delta$ 1, pleckstrin-C; **2\***: ArhGAP9, AKT1, ARNO,  $\beta$ -spectrin, PEPP1. Modes adopted by only one domain e.g. for DAPP1 and BTK while loosely bound are not shown. PIP is shown in magenta; the membrane is shown in grey with phosphate groups shown explicitly in light (POPC) or dark (POPS) grey. Protein is shown by the cartoon representation of the aligned crystal structure, with the main loops that bound the A- and C- sites are labelled.

Preference for these different binding orientations on to the membrane can be explained by the distribution of positively charged residues across loops corresponding to the A or C sites. PH domains with a large number of positive/polar residues in the  $\beta 3$ - $\beta 4$  loop (e.g. PLC $\delta 1$ , BTK and  $\beta$ -spectrin; Supplementary Figure S2) bind in an orientation that allows PIP to align with this loop when at the C-site ('4' in Figure 7), rather than with the  $\beta 1$ - $\beta 2$  loop as in the more common orientation ('1' in Figure 7). Strongly interacting residues are also observed in this region for kindlin-2; however, this loop is relatively long and unstructured, and hence flexible, in kindlin-2 (Figure 1), allowing these additional interactions without a change in overall orientation of the PH domain relative to the bilayer.

Additional charges along the 'front' face of the PH domain (at the end of the  $\beta 1$ - $\beta 2$  loop for AhrGAP9,  $\beta$ -spectrin and pleckstrin-C, or the  $\beta 5$ - $\beta 6$  loop for DAPP1, AKT1, ASAP1; Supplementary Figure S2) result in binding modes in which the PH domain rotates forward so PIP is in better contact with these residues; this may occur for PIP binding in the A-site ('5' in Figure 7) or C-site ('3' in Figure 7).

In most cases, the same patterns of interaction modes are seen across all simulations for a given PH domain. However, BTK showed variations in the number and depth of the energy wells across the four simulations. This may be due to the restraints orthogonal to the membrane applied to assist in reaching sufficient sampling; in a more complicated binding energy landscape, if the two starting structures are displaced these restraints may result in sampling slices from the full energy landscape in which the favourability of binding modes differs. This effect may also explain the relatively large error between repeats for DAPP1. However, the good agreement between the sets of profiles for the majority of PH domains suggests this was not an issue in most cases.

#### *Structural basis of affinity and selectivity*

The free energies of interaction with PIP-containing membranes can be related back to structural features of the PH domains. The identity of the PIP-binding site appears to be a good indicator of affinity, with PH domains showing higher affinities being those with more C-site interactions (e.g. Group III; Figure 8A), while a greater degree of A-site over other interactions correlates with weaker binding (Figure 8B). The generally greater strength of C-site interactions is likely due to the more 'closed' nature of this site, such that the PIP molecule sits inside the curve of the  $\beta 1/\beta 2$  loop thus allowing a greater number of interacting residues. In contrast the A-site, on the opposite side of this loop, is more open.

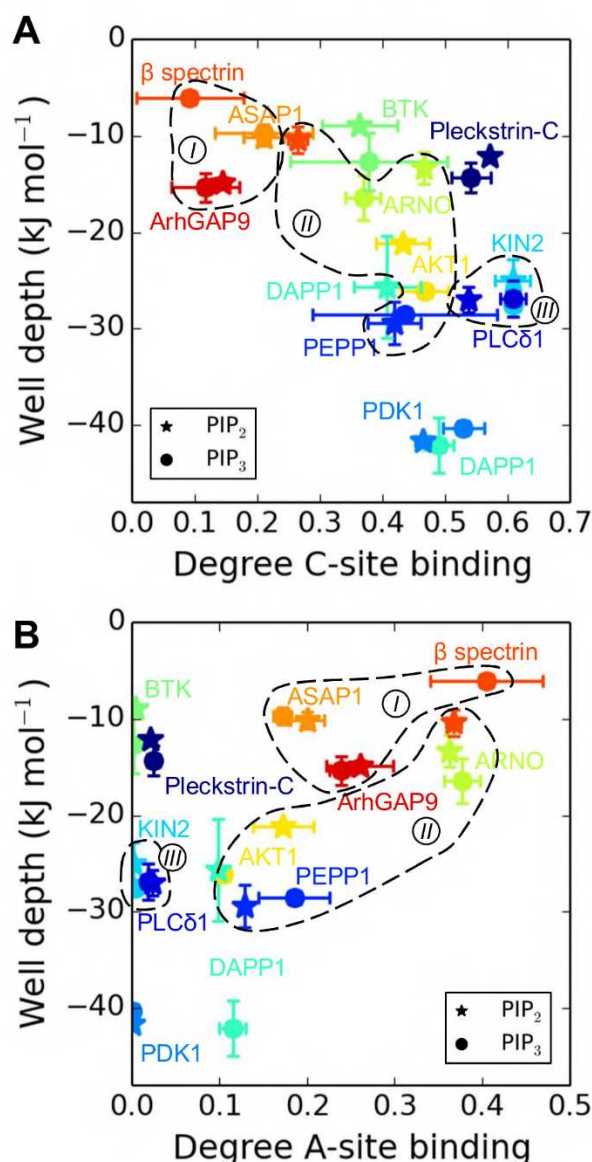


**Figure 8.** Average well depth for each PH-PIP system studied against **A.** degree of C-site binding or **B.** degree of A site binding. ‘Degree of C-site binding’ is defined as the fraction of frames with at least two C-site contacts and a binding angle  $-50-10^0$  of all frames where any two contacts are observed. ‘Degree of A-site binding’ is the fraction of non-C interacting frames with at least two A-site contacts and a PIP binding angle between  $0-60^0$ .

Of the three domains that exhibit selective binding in this study (i.e.  $\beta$ -spectrin, DAPP1 and AKT1), selectivity of  $\beta$ -spectrin can most clearly be linked with the binding mode. For  $\text{PIP}_3$ ,  $\beta$ -spectrin shows largely A-site interactions when tightly bound, while  $\text{PIP}_2$  is able to interact more strongly with the C-site (Figure 6), seen in the PMF profiles as an additional deeper well (Figure 3, Supplementary Figure S1).  $\beta$ -spectrin binds  $\text{PIP}_3$  in the orientation so that the PIP molecule is aligned along the  $\beta 3$ - $\beta 4$  loop (‘4’ in Figure 7). This loop extends away from the C-site at a larger angle than for other domains that bind in this orientation, leading to a relatively shallow binding site

less accommodating for the larger headgroup of PIP<sub>3</sub>. Consequently, PIP<sub>2</sub> interactions are favoured over PIP<sub>3</sub> for this domain (Figure 4 and above).

DAPP1 was observed to be highly PIP<sub>3</sub> selective. DAPP1 interacts with PIP when tightly bound with two possible orientations ('1' and '3' in Figure 7); the latter allows additional electrostatic interactions and is observed to a greater extent with PIP<sub>3</sub>, perhaps due to the higher charge, leading to the observed selectivity. AKT1 was also observed to be PIP<sub>3</sub> selective, though there is no clear difference in binding mode between PIP<sub>2</sub> and PIP<sub>3</sub>. This selectivity may also be simply the result of the increased charge of the PIP<sub>3</sub> molecule. It is not clear why DAPP1 exhibits a much greater degree of selectivity than any other domain.

Overall, given the low degree of selectivity observed here, it remains difficult to isolate clear trends which determining PIP<sub>2</sub> vs. PIP<sub>3</sub> selectivity across the PH family, though interactions with PIP<sub>3</sub> do appear in general to be more energetically favourable (Figure 4B), as would be expected given its greater charge. Determinants of selective binding may be revealed following investigation of a more extended set of PH domains via simulations.

#### *Dual binding at the canonical and atypical sites*

Our simulations lead to the question of whether a PH domain can interact with a membrane via more than one PH/PIP interaction. We have demonstrated A-site interactions for several PH domains – most clearly for ArhGAP9, ASAP1, and  $\beta$ -spectrin but also for AKT1, ARNO and PEPP1. Previously, structural studies had suggested interaction of PIP at both sites only for ASAP1<sup>23</sup>, whilst computational studies have additionally suggested that interactions with both binding sites are possible for e.g. GRP1<sup>39</sup>, Dok7<sup>41</sup> and ACAP1<sup>43</sup>.

Weaker binding correlates with fewer C-site interactions, but also with more A-site interactions (Figure 8), suggesting that the A-site may 'compensate' for weaker C-site interactions. In particular, the presence of the A-site may enable binding of *multiple* PIP lipid molecules to a single PH domain. In most of the binding modes (with the exception of mode '4'), both the A- and C-sites are presented towards the membrane (Figure 7), making simultaneous binding of a PH domain to two PIP molecules possible.

Such dual-binding interactions of a PH domain is expected to significantly increase the binding free energy of a PH domain to a PIP-containing membrane. We tested this for the Grp1 PH domain (Figure 9). Thus, the presence of an additional PIP molecule bound at the A-site was found to nearly double the well depth calculated from umbrella sampling compared to a single PIP bound at the C-site. This would correspond to a  $K_D$  of  $\sim 10$   $\mu$ M for the two PIP simulation compared to 5 mM for the single PIP simulation and 1  $\mu$ M or less from experimental estimates. This suggests that

additional, less specific, nanoclustering of PIP molecules around a PH domain (as seen in a number of simulation studies<sup>41; 42; 43; 62</sup>) is likely to contribute a further term to the experimentally observed binding free energy.

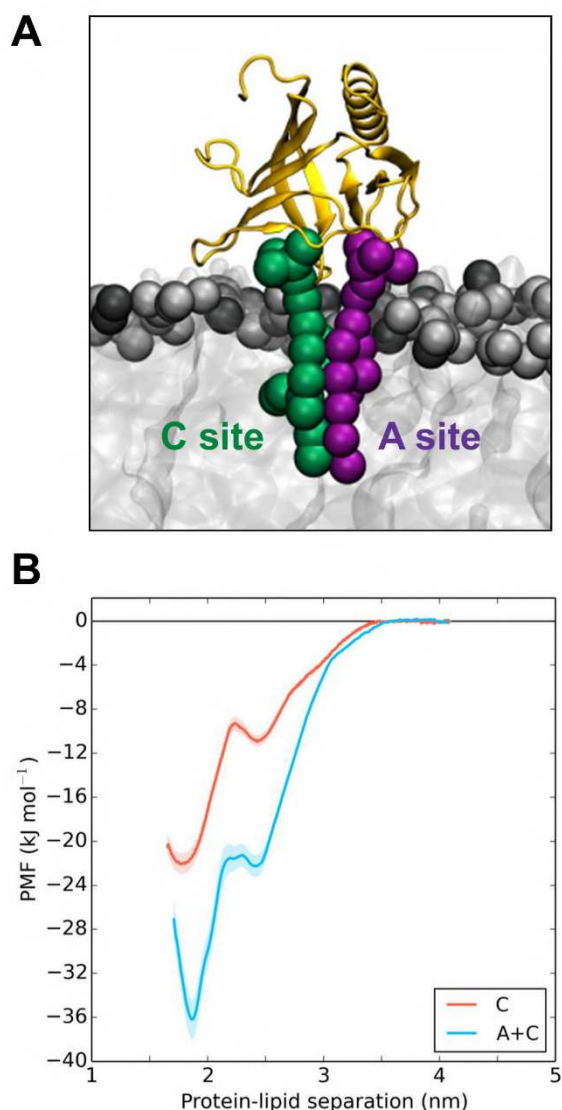


**Figure 9.** **A.** The GRP1 PH domain with PIP<sub>3</sub> molecules bound both the C- and A-sites. The aligned crystal structure of GRP1-PH is shown in cartoon representation in yellow; the PIPs bound to the C and A sites are shown in green and purple, respectively. The membrane is shown in grey with headgroups of POPC (light grey) and POPS (dark grey) shown explicitly. **B.** PMF profiles corresponding to the PH domain of GRP1 binding to either a single PIP<sub>3</sub> molecule initially at the C-site (red) or to two PIPs, initially at the C- and A-sites (blue). A profile for GRP1-PH binding to PIP<sub>3</sub> was obtained from a previous study, along with a structure of GRP1-PH binding to a membrane containing multiple PIP<sub>3</sub> lipids, including one in each the A and C sites. All but the PIPs in these sites were replaced by POPC lipids, and an umbrella sampling simulation performed as outlined in Methods, with both PIPs restrained.

We also note that those domains for which the difference between experimental and computational  $\Delta G_o$  values (Figure 4C) is greatest tend to be those with more favourable A-site interactions (i.e. Group I domains, AhrGAP9 and  $\beta$ -spectrin) and so for which one would expect to see a substantive increase when multiple PIPs were present. Those PH domains for which the computational (single PIP) estimates are closer to (within two-fold) the experimental range tend to be those for which strong A-site interactions were not observed (i.e. kindlin-2 and PLC $\delta$ 1 of ‘Group III’, and DAPP1 and PDK1 of ‘Group IV’), and so would not be expected to show as significant an increase. This further suggests that the presence of two PIP interaction sites may play a role in directing the binding of PH domains to membranes. We note, however, that for some PH domains e.g. ARNO that exhibit a strong PIP binding to the C-site, the computational and the experimental difference is comparable to the difference for PH domains with more favourable A-site interactions. Therefore, studies with a larger set of PH domain structures may be required to further support our hypothesis.

## CONCLUSIONS

We have used an umbrella sampling/coarse-grained molecular dynamics approach to calculate one-dimensional free energy profiles for the binding of 12 different PH domains to model membranes containing either a PI(4,5)P<sub>2</sub> or PI(3,4,5)P<sub>3</sub> lipid molecule. This allows us, for the first time, to obtain a molecular energetic understanding of the complexities of the interactions of the PH domains with PIP molecules in membranes.

A range of affinities, selectivity (between PIP<sub>2</sub> and PIP<sub>3</sub>), and binding modes were observed. These are related to structural and sequence differences between the different PH domain species. We propose a classification scheme for PH domains according to the relative strength of interaction modes involving the ‘canonical’ and/or the ‘atypical’ binding sites. This correlates with the relative strength of interactions with a single PIP molecule.

This and previous computational studies (see e.g. <sup>39; 40; 41; 43; 54; 66</sup>) indicate the ability of many PH domains to interact specifically with multiple PIP molecules through both their A and C sites. In addition to enhancing the avidity of the PH domain for the target membrane, the presence of two distinct interaction sites may also ensure binding in a ‘productive’ orientation and, being in general more favourable at larger protein-lipid separations, may also play a role in the initial membrane recruitment and encounter process from which the tight ‘productive’ binding orientation is then reached.

It is also possible that the two sites may preferentially interact with different lipids, including non-PIP species, allowing more targeted recruitment to membranes only where both species are present.

Indeed, of those domains studied here, experimental studies have suggested that the A-sites of AKT1<sup>67</sup> and PDK1<sup>68</sup> may bind phosphatidylserine. Large-scale studies have suggested this ‘coincidence detection’ plays an important role in the targeting of a large number of PH and lipid binding domains in general<sup>69;70</sup>.

It is perhaps helpful to comment on the use of a coarse-grained representation in these simulations. Whilst the use of coarse-grained simulations implies some approximations in the protein and the lipids, this method allows access to larger timescales. This enables improved sampling and hence statistically meaningful free energy profiles. Thus, it has been shown that CG simulations combined with umbrella sampling can yield converged estimates of free energies of protein-lipid interactions within a bilayer<sup>52</sup>. A more general question, which we have tried to address by comparison with a range of experimental data for PH domains, is whether the MARTINI forcefield correctly estimates the free energy of interaction of proteins with the lipid bilayer/water interface. Simulations of model systems have suggested that MARTINI may over-estimate the strength of interaction of a hydrophobic peptide with the membrane interface<sup>71</sup>. In contrast, in the current study comparison with experiment suggests the strength of interaction of the more structurally complex PH domain with the surface of a mixed lipid bilayer seems, if anything, to be underestimated. Further simulation studies of a wider range of membrane-binding proteins would help to cast further light on this, and comparison with experimental data will be central to such studies. Whilst atomistic umbrella sampling simulations, as recently used to study the PH-domain of ACAP1 binding PIP-containing membranes<sup>43</sup>, may offer a higher resolution picture of free energy landscapes, the considerable challenges of achieving convergence may limit comparisons of multiple systems. The same challenges apply with the use of the polarizable water model instead of the simple coarse-grained water particle used in this study. As we have shown in our previous studies with the GPR1 PH domain<sup>39</sup>, the use of the polarizable MARTINI water model alters the depth of the PMF minimum and increases the complexity of the energy landscape but it needs substantially more time in order to reach convergence. In the absence of fully sampled atomistic PMFs against which to calibrate the coarse grained results we have therefore elected to employ the simpler (i.e. non-polarizable) MARTINI water model.

In summary, this study provides a first systematic comparison of the molecular energetics of PH domain protein-membrane interactions across a family of related proteins, revealing unexpected complexities, and providing a proof-of-principle for the application of this approach to other families of peripheral membrane proteins.

## METHODS

All simulations were performed using Gromacs 4.6.5<sup>72</sup> and the Martini 2.1 force field<sup>73; 74</sup>. Simulation timestep was 20 fs. Coordinates were written out every 400 ps; during umbrella sampling simulations, reaction coordinate values were written out every 20 ps. Coulomb interactions were shifted to zero between 0-1.2 nm, and Lennard-Jones interactions between 0.9-1.2 nm. The nearest neighbour list was updated every 10 steps. A Berendsen thermostat and barostat (coupling constant 1 ps, compressibility  $5 \times 10^{-6} \text{ bar}^{-1}$ ) were applied to maintain temperature and pressure at 323 K and 1 bar, respectively. The LINCS algorithm<sup>75</sup> was used to constrain bond lengths. Periodic boundary conditions in *xyz* were applied. Semi-isotropic pressure coupling was used.

### *Initial structures*

Atomistic structures of PH domains bound to PIP-containing membranes were generated by obtaining the best-fit alignment between phosphorous atoms of PIP-analogues bound in the corresponding PDB entry structures and a PIP<sub>2</sub> or PIP<sub>3</sub> lipid molecule embedded in a pre-equilibrated POPC:POPS 80:20 bilayer. This bilayer measured 11.3 x 11.3 nm<sup>2</sup> and contained a total of 384 lipids (306 POPC, 77 POPS and one PIP<sub>2</sub> or PIP<sub>3</sub>). For some domains (e.g. ASAP1 A-site), the PIP analogue was found to be ‘upside down’ in the crystal structure (see e.g.<sup>42</sup> for details); in these cases, pairs of atoms to be aligned were chosen for a more appropriate orientation.

These structures were then converted to a coarse-grained (MARTINI<sup>73; 74</sup>) representation, solvated in a 11.3 x 11.3 x 15 nm<sup>3</sup> water box, and 0.15 M neutralising ions (NaCl) added. The structure was energy minimised and equilibrated for 5 ns. This formed the ‘crystal’ starting structure.

A 1  $\mu\text{s}$  simulation, in which no restraints were applied between protein and PIP, was performed. The positions of bound PIP molecules relative to the PH domain throughout the simulation were clustered, and a representative structure selected. This was the ‘simulation’ starting structure.

### *Umbrella Sampling (US) and PMF profiles*

From each initial structure, a steered molecular dynamics simulation was performed in which the PH domain was pulled away perpendicular to the membrane surface at 0.001 nm ps<sup>-1</sup> ( $k = 1000 \text{ kJ mol}^{-1} \text{ nm}^{-2}$ ) for a total distance of 2.6 nm. A 1000 kJ mol<sup>-1</sup> nm<sup>-2</sup> restraint was applied to the 1' phosphate of the PIP to prevent it leaving the membrane. From this trajectory, snapshots were extracted of different protein-lipid separation, measured from the protein centre-of-mass to PIP 1' phosphate, at 0.1 nm intervals for the first 2 nm and 0.2 nm thereafter. These snapshots were then the starting structures used for a set of US ‘windows’, in which protein-lipid distance was restrained

( $k = 1000 \text{ kJ mol}^{-1} \text{ nm}^{-2}$ ). Centre-of-mass restraints were also applied in the orthogonal directions ( $k = 100 \text{ kJ mol}^{-1} \text{ nm}^{-2}$ ) to reduce the volume available to sample and so speed convergence. The PIP restraint was maintained; this restraint was found to not significantly impact the final result in the case of GRP1<sup>36</sup>. Each window was simulated for 2+  $\mu\text{s}$  until the convergence of the profile, assessed by calculating PMFs over a sliding 0.2  $\mu\text{s}$  window. Subsequent analysis excludes time before convergence. In some cases, additional windows were added at the start or end, to ensure the profile covered the minimum and reached a plateau at large separation. Full and detailed information about the umbrella sampling simulations are included in Table S11.

PMF profiles were calculated using the Grossfield WHAM implementation (<http://membrane.urmc.rochester.edu/content/wham>) and shifted so the value in bulk was  $0 \text{ kJ mol}^{-1}$ . Errors were obtained from bootstrap analysis using 200 bootstraps. Convergence of the simulations is examined in Supplementary Figure S7.

To determine average values in subsequent analysis, the effect of the umbrella restraints was accounted for by a weighting factor:

$$\exp\left(\frac{U - F}{RT}\right) \quad (1)$$

calculated for each simulation frame, where  $U$  is the potential energy of the frame due to the umbrella restraint of the window it is from,  $F$  is the normalisation factor of that window,  $R$  is the gas constant and  $T$  the temperature.

#### *Calculation and comparison of binding free energies*

As described in reference<sup>53</sup>, the standard binding free energy from a 1D PMF  $W_R(z)$  (shifted so the energy well corresponds to  $0 \text{ kJ mol}^{-1}$ ) in which restraints  $k_{xy}$  are applied orthogonal to the reaction coordinate is given by:

$$\Delta G_{bind}^{\circ} = \Delta W_R - RT \ln \left( \frac{2\pi RT}{V^{\circ} k_{xy}} \int_{bound} \exp\left(\frac{-W_R(z)}{RT}\right) dz \right) + \Delta G_R \quad (2)$$

The integral is performed over the ‘bound’ region, from the well until the bulk-region plateau is reached.  $\Delta W_R$  is the well depth of the profile,  $R$  is the gas constant,  $T$  is the temperature,  $V^{\circ}$  is the standard state volume and  $\Delta G_R$  accounts for the effects of the lateral restraints, calculated as:

$$\Delta G_R = RT \ln \left( \exp\left(\frac{-k_{xy}(\Delta x^2 + \Delta y^2)}{2RT}\right) \right)_{k_{xy}=0} \quad (3)$$

$\Delta x$  and  $\Delta y$  are displacements of the protein centre of mass from the location of the orthogonal restraint minimum, averaged over a simulation in which no restraints were applied.

$\Delta G_{bind}^{\circ}$  values were calculated for each profile using Equation 2, with the unrestrained simulation used to calculate  $G_R$ .  $\Delta G_{bind}$  is related to the dissociation constant  $K_D$  by:

$$\Delta G_{bind} = RT \ln \frac{K_D}{c^{\ominus}} \quad (4)$$

This relation was used to calculate  $\Delta G_{bind}^{\circ}$  from reported experimental values. If temperature was not reported, a standard temperature of 298 K was assumed. Fold-selectivities were calculated from computational results by taking the ratio of equivalent  $K_D$  values calculated using Equation 4.

### *Binding site analysis*

A residue was defined to be in contact with PIP when any sidechain particle of the residue was within 0.6 nm of a PIP phosphate particle. Structure-based sequence alignment of PH domains was performed using the VMD <sup>76</sup> plugin MultiSeq <sup>77</sup>, and A- and C-site residues identified as those equivalent to a contact observed in any crystal structure for PIP bound in the appropriate site. Relative A/C contacts was determined by counting the number of A- and C-site residues in contact with PIP in each frame, scaling each by the total number of A/C site residues with sidechain particles present for the particular PH domain.

The PIP-binding angle was measured by first aligning the proteins to a reference structure. The angle formed between the centre of mass of the phosphate particles of the PIP headgroup, the centre of mass of the PH domain and the vertical axis passing through the protein centre of mass was then measured (see Figure 5). We note that use of an ENM in the CG simulations restrains the PH domain so it cannot undergo any substantive conformational changes during the simulations.

Taking greater than two contacts as a ‘bound state’, the ‘degree of C-site binding’ was calculated as the fraction of bound-state frames in which the interaction is with the C-site (at least two C-site interactions and a binding angle between -50 and 10°). ‘Degree of A-site binding’ was calculated as the fraction of non-C binding frames in which the interaction was with the A-site (at least two A-site interactions and a binding angle between 0 and 60°).

### *Binding mode analysis*

The orientation of a PH domain relative to the membrane was measured by aligning (in the plane of the membrane i.e. the  $xy$  plane) the PH domain in each frame with a reference structure, then calculating the rotation matrix between the structures and taking the  $R_{ZZ}$  component. Binding energy landscapes along the PIP binding angle and membrane orientation were calculated from all simulations in each group (I – IV). These landscapes were then normalised and added to obtain a combined landscape for all simulations.

### *AKT1-PH mutant*

The E17K mutant of AKT1 was generated using the Mutator plugin of VMD. PMF profiles, using a ‘crystal’ initial structure, were generated for binding with PIP<sub>2</sub> and PIP<sub>3</sub> as described above.

*GRP1-PH binding to one or two PIPs*

A profile for GRP1-PH binding to PIP<sub>3</sub> was obtained from a previous study<sup>39</sup>, along with a structure of GRP1-PH binding to a membrane containing multiple PIP<sub>3</sub> lipids, including one in each the A and C sites. All but the two PIP molecules in these sites were replaced by POPC lipids, and an umbrella sampling simulation performed as outlined above, with both PIPs restrained.

**ACKNOWLEDGEMENTS.**

A.C.K. and M.S.P.S. were funded by the Wellcome Trust and the BBSRC. F.B.N. was supported by the Clarendon Fund and Lincoln College, University of Oxford. We acknowledge the EPSRC and the UK High-End Computing Consortium for Biomolecular Simulation for time on the ARCHER supercomputer.

## REFERENCES

1. Cho, W. & Stahelin, R. V. (2005). Membrane-protein interactions in cell signaling and membrane trafficking. *Ann. Rev. Biophys. Biomol. Str.* **34**, 119-151.
2. Lemmon, M. A. (2008). Membrane recognition by phospholipid-binding domains. *Nat. Rev. Mol. Cell Biol.* **9**, 99-111.
3. Moravcevic, K., Oxley, Camilla L. & Lemmon, Mark A. (2012). Conditional peripheral membrane proteins: Facing up to limited specificity. *Structure* **20**, 15-27.
4. Kutateladze, T. G. (2010). Translation of the phosphoinositide code by PI effectors. *Nature Chem. Biol.* **6**, 507-513.
5. Di Paolo, G. & De Camilli, P. (2006). Phosphoinositides in cell regulation and membrane dynamics. *Nature* **443**, 651-657.
6. Stahelin, R. V., Scott, J. L. & Frick, C. T. (2014). Cellular and molecular interactions of phosphoinositides and peripheral proteins. *Chem. Phys. Lipids* **182**, 3-18.
7. Cantley, L. C. (2002). The phosphoinositide 3-kinase pathway. *Science* **296**, 1655-1657.
8. DiNitto, J. P. & Lambright, D. G. (2006). Membrane and juxtamembrane targeting by PH and PTB domains. *Biochim. Biophys. Acta* **1761**, 850-867.
9. Wymann, M. P. & Schneider, R. (2008). Lipid signalling in disease. *Nat. Rev. Mol. Cell Biol.* **9**, 162-176.
10. Lindvall, J. M., Blomberg, K. E. M., Valiaho, J., Vargas, L., Heinonen, J. E., Berglof, A., Mohamed, A. J., Nore, B. F., Vihinen, M. & Smith, C. I. E. (2005). Bruton's tyrosine kinase: cell biology, sequence conservation, mutation spectrum, siRNA modifications, and expression profiling. *Immunol. Rev.* **203**, 200-215.
11. Carpten, J. D., Faber, A. L., Horn, C., Donoho, G. P., Briggs, S. L., Robbins, C. M., Hostetter, G., Boguslawski, S., Moses, T. Y., Savage, S., Uhlik, M., Lin, A., Du, J., Qian, Y.-W., Zeckner, D. J., Tucker-Kellogg, G., Touchman, J., Patel, K., Mousses, S., Bittner, M., Schevitz, R., Lai, M.-H. T., Blanchard, K. L. & Thomas, J. E. (2007). A transforming mutation in the pleckstrin homology domain of AKT1 in cancer. *Nature* **448**, 439-444.
12. Sudhakar, C. G., Haney, R. M., Xue, Y. & Stahelin, R. V. (2008). Cellular membranes and lipid-binding domains as attractive targets for drug development. *Curr. Drug Targets* **9**, 603-613.
13. Ryckbosch, S. M., Wender, P. A. & Pande, V. S. (2017). Molecular dynamics simulations reveal ligand-controlled positioning of a peripheral protein complex in membranes. *Nature Comms.* **8**, doi:10.1038/s41467-016-0015-8.
14. Scott, J. L., Musselman, C. A., Adu-Gyamfi, E., Kutateladze, T. G. & Stahelin, R. V. (2012). Emerging methodologies to investigate lipid-protein interactions. *Integrat. Biol.* **4**, 247-258.
15. Ferguson, K. M., Lemmon, M. A., Schlessinger, J. & Sigler, P. B. (1995). Structure of the high affinity complex of inositol trisphosphate with a phospholipase C pleckstrin homology domain. *Cell* **83**, 1037-1046.
16. Hyvönen, M., Macias, M. J., Nilges, M., Oschkinat, H., Saraste, M. & Wilmanns, M. (1995). Structure of the binding site for inositol phosphates in a PH domain. *EMBO J.* **19**, 4676-4685.
17. Lietzke, S. E., Bose, S., Cronin, T., Klarlund, J., Chawla, A., Czech, M. P. & Lambright, D. G. (2000). Structural basis of 3-phosphoinositide recognition by pleckstrin homology domains. *Mol. Cell* **6**, 385-394.
18. Ferguson, K. M., Kavran, J. M., Sankaran, V. G., Fournier, E., Isakoff, S. J., Skolnik, E. Y. & Lemmon, M. A. (2000). Structural basis for discrimination of 3-phosphoinositides by pleckstrin homology domains. *Mol. Cell* **6**, 373-384.
19. Komander, D., Fairservice, A., Deak, M., Kular, G. S., Prescott, A. R., Peter Downes, C., Safrany, S. T., Alessi, D. R. & van Aalten, D. M. F. (2004). Structural insights into the regulation of PDK1 by phosphoinositides and inositol phosphates. *EMBO J.* **23**, 3918-3928.

20. Cronin, T., DiNitto, J. P., Czech, M. P. & Lambright, D. G. (2004). Structural determinants of phosphoinositide selectivity in splice variants of Grp1 family PH domains. *EMBO J.* **7**, 1157-1166.
21. Jackson, S., Zhang, Y., Haslam, R. & Junop, M. (2007). Structural analysis of the carboxy terminal PH domain of pleckstrin bound to D-myo-inositol 1,2,3,5,6-pentakisphosphate. *BMC Struct. Biol.* **7**, 80.
22. Liu, J., Fukuda, K., Xu, Z., Ma, Y.-Q., Hirbawi, J., Mao, X., Wu, C., Plow, E. F. & Qin, J. (2011). Structural basis of phosphoinositide binding to kindlin-2 protein pleckstrin homology domain in regulating integrin activation. *J. Biol. Chem.* **286**, 43334-43342.
23. Jian, X., Tang, W.-K., Zhai, P., Roy, Neeladri S., Luo, R., Gruschus, James M., Yohe, Marielle E., Chen, P.-W., Li, Y., Byrd, R. A., Xia, D. & Randazzo, Paul A. (2015). Molecular basis for cooperative binding of anionic phospholipids to the PH domain of the Arf GAP ASAP1. *Structure* **23**, 1977-1988.
24. Anand, K., Maeda, K. & Gavin, A.-C. (2012). Structural analyses of the Slm1-PH domain demonstrate ligand binding in the non-canonical site. *PLoS ONE* **7**, e36526.
25. Maroun, C. R., Moscatello, D. K., Naujokas, M. A., Holgado-Madruga, M., Wong, A. J. & Park, M. (1999). A conserved inositol phospholipid binding site within the pleckstrin homology domain of the Gab1 docking protein is required for epithelial morphogenesis. *J. Biol. Chem.* **274**, 31719-31726.
26. Gorai, S., Paul, D., Haloi, N., Borah, R., Santra, M. K. & Manna, D. (2016). Mechanistic insights into the phosphatidylinositol binding properties of the pleckstrin homology domain of lamellipodin. *Molec. Biosyst.* **12**, 747-757.
27. Ceccarelli, D. F. J., Blasutig, I. M., Goudreault, M., Li, Z., Ruston, J., Pawson, T. & Sicheri, F. (2007). Non-canonical interaction of phosphoinositides with Pleckstrin Homology domains of Tiam1 and ArhGAP9. *J. Biol. Chem.* **282**, 13864-13874.
28. Salim, K., Bottomley, M. J., Querfurth, E., Zvelebil, M. J., Gout, I., Scaife, R., Margolis, R. L., Gigg, R., Smith, C. I. E., Driscoll, P. C., Waterfield, M. D. & Panayotou, G. (1996). Distinct specificity in the recognition of phosphoinositides by the pleckstrin homology domains of dynamin and Bruton's tyrosine kinase. *EMBO J.* **15**, 6241-6250.
29. Zheng, J., Cahill, S. M., Lemmon, M. A., Fushman, D., Schlessinger, J. & Cowburn, D. (1996). Identification of the binding site for acidic phospholipids on the PH domain of dynamin: Implications for stimulation of GTPase activity. *J. Molec. Biol.* **255**, 14-21.
30. Prashek, J., Truong, T. & Yao, X. L. (2013). Crystal structure of the pleckstrin homology domain from the ceramide transfer protein: Implications for conformational change upon ligand binding. *PLoS One* **8**.
31. Harlan, J. E., Hajduk, P. J., Yoon, H. S. & Fesik, S. W. (1994). Pleckstrin homology domains bind to phosphatidylinositol-4,5-bisphosphate. *Nature* **371**, 168-170.
32. Landgraf, K. E., Pilling, C. & Falke, J. J. (2008). Molecular mechanism of an oncogenic mutation that alters membrane targeting: Glu17Lys modifies the pip lipid specificity of the Akt1 PH Domain. *Biochemistry* **47**, 12260-12269.
33. Frech, M., Andjelkovic, M., Ingley, E., Reddy, K. K., Falck, J. R. & Hemmings, B. A. (1997). High affinity binding of inositol phosphates and phosphoinositides to the Pleckstrin homology domain of RAC protein kinase B and their influence on kinase activity. *J. Biol. Chem.* **272**, 8474-8481.
34. Kalli, A. C. & Sansom, M. S. P. (2014). Interactions of peripheral proteins with model membranes as viewed by molecular dynamics simulations. *Biochem. Soc. Trans.* **42**, 1418-1424.
35. Hedger, G. & Sansom, M. S. P. (2016). Lipid interaction sites on channels, transporters and receptors: recent insights from molecular dynamics simulations. *Biochim. Biophys. Acta* **1858**, 2390-2400.

36. Lumb, C. N., He, J., Xue, Y., Stansfeld, P. J., Stahelin, R. V., Kutateladze, T. G. & Sansom, M. S. P. (2011). Biophysical and computational studies of membrane penetration by the GRP1 pleckstrin homology domain. *Structure* **19**, 1338-1346.
37. Rosen, S. A. J., Gaffney, P. R. J., Spiess, B. & Gould, I. R. (2012). Understanding the relative affinity and specificity of the pleckstrin homology domain of protein kinase B for inositol phosphates. *Phys. Chem. Chem. Phys.* **14**, 929-936.
38. Lai, C.-L., Srivastava, A., Pilling, C., Chase, A. R., Falke, J. J. & Voth, G. A. (2013). Molecular mechanism of membrane binding of the GRP1 PH domain. *J. Mol. Biol.* **425**, 3073-3090.
39. Naughton, F. B., Kalli, A. C. & Sansom, M. S. P. (2016). Association of peripheral membrane proteins with membranes: Free energy of binding of GRP1 PH domain with PIP-containing model bilayers. *J. Phys. Chem. Lett.* **7**, 1219-1224.
40. Ni, T., Kalli, A. C., Naughton, F. B., Yates, L. A., Naneh, O., Kozorog, M., Anderluh, G., Sansom, M. S. P. & Gilbert, R. J. C. (2017). Structure and lipid binding properties of the kindlin-3 pleckstrin homology domain. *Biochem. J.* **474**, 539–556.
41. Buyan, A., Kalli, A. C. & Sansom, M. S. P. (2016). Multiscale simulations suggest a mechanism for the association of Dok7 with PIP-containing membranes. *PLoS Comp. Biol.* **12**, e1005028.
42. Yamamoto, E., Kalli, A. C., Yasuoka, K. & Sansom, M. S. P. (2016). Interactions of pleckstrin homology domains with membranes: adding back the bilayer via high throughput molecular dynamics. *Structure* **24**, 1421-1431.
43. Chan, K. C., Lu, L., Sun, F. & Fan, J. (2017). Molecular details of the PH domain of ACAP1<sup>BAR-PH</sup> protein binding to PIP-containing membrane. *J. Phys. Chem. B* **121**, 3586–3596.
44. Kuang, G. L., Bulone, V. & Tu, Y. Q. (2016). Computational studies of the binding profile of phosphoinositide PtdIns (3,4,5) P-3 with the pleckstrin homology domain of an oomycete cellulose synthase. *Sci. Rep.* **6**.
45. Jaud, S., Tobias, D. J., Falke, J. J. & White, S. H. (2007). Self-induced docking site of a deeply embedded peripheral membrane protein. *Biophys. J.* **92**, 517–524.
46. Lai, C.-L., Landgraf, K. E., Voth, G. A. & Falke, J. J. (2010). Membrane docking geometry and target lipid stoichiometry of membrane-bound PKC $\alpha$  C2 domain: A combined molecular dynamics and experimental study. *J. Mol. Biol.* **402**, 301-310.
47. Kalli, A. C., Devaney, I., Sansom, M.S.P. (2014). Interactions of phosphatase and tensin homologue (PTEN) proteins with phosphatidylinositol phosphates: insights from molecular dynamics simulations of PTEN and voltage sensitive phosphatase. *Biochem.* **53**, 1724-1732.
48. Roux, B. (1995). The calculation of the potential of mean force using computer simulations. *Comp. Physics Comm.* **91**, 275-282.
49. Marrink, S. J., de Vries, A. H. & Mark, A. E. (2004). Coarse grained model for semiquantitative lipid simulations. *J. Phys. Chem. B* **108**, 750-760.
50. Arnarez, C., Marrink, S. J. & Periole, X. (2013). Identification of cardiolipin binding sites on cytochrome c oxidase at the entrance of proton channels. *Sci. Rep.* **3**, 1263.
51. Hedger, G., Rouse, S. L., Domański, J., Chavent, H., Koldsø, H. & Sansom, M. S. P. (2016). Lipid loving ANTs: molecular simulations of cardiolipin interactions and the organization of the adenine nucleotide translocase in model mitochondrial membranes. *Biochemistry* **55**, 6238–6249.
52. Domański, J., Hedger, G., Best, R., Stansfeld, P. J. & Sansom, M. S. P. (2017). Convergence and sampling in determining free energy landscapes for membrane protein association. *J. Phys. Chem. B.* **121**, 3364–3375.
53. Doudou, S., Neil, A. & Henchman, R. H. (2009). Standard free energy of binding from a one-dimensional potential of mean force. *J. Chem. Theor. Comput.* **5**, 909-918.
54. Lenoir, M., Kufareva, I., Abagyan, R. & Overduin, M. (2015). Membrane and Protein Interactions of the Pleckstrin Homology Domain Superfamily. *Membranes* **5**, 646-663.

55. Manna, D., Albanese, A., Park, W. S. & Cho, W. (2007). Mechanistic basis of differential cellular responses of phosphatidylinositol 3,4-bisphosphate- and phosphatidylinositol 3,4,5-trisphosphate-binding pleckstrin homology domains. *J. Biol. Chem.* **282**, 32093-32105.
56. He, J., Haney, R. M., Vora, M., Verkhusha, V. V., Stahelin, R. V. & Kutateladze, T. G. (2008). Molecular mechanism of membrane targeting by the Grp1 PH domain. *J. Lipid Res.* **49**, 1807-1815.
57. Uekama, N., Sugita, T., Okada, M., Yagisawa, H. & Tuzi, S. (2007). Phosphatidylserine induces functional and structural alterations of the membrane-associated pleckstrin homology domain of phospholipase C- $\delta$ 1. *FEBS J.* **274**, 177-187.
58. Yates, L. A., Lumb, C. N., Brahme, N. N., Bird, L. E., De Colibus, L., Owens, R. J., Calderwood, D. A., Sansom, M. S. P. & Gilbert, R. J. C. (2012). Structural and functional characterisation of the kindlin-1 pleckstrin homology domain. *J. Biol. Chem.* **287**, 43246–43261.
59. Pilling, C., Landgraf, K. E. & Falke, J. J. (2011). The GRP1 PH domain, like the AKT1 PH domain, possesses a sentry glutamate residue essential for specific targeting to plasma membrane PI(3,4,5)P<sub>3</sub>. *Biochemistry* **50**, 9845-9856.
60. Garcia, P., Gupta, R., Shah, S., Morris, A. J., Rudge, S. A., Scarlata, S., Petrova, V., McLaughlin, S. & Rebecchi, M. J. (1995). The pleckstrin homology domain of phospholipase C- $\delta$ 1 binds with high affinity to phosphatidylinositol 4,5-bisphosphate in bilayer membranes. *Biochemistry* **34**, 16228-16234.
61. Flesch, F. M., Yu, J. W., Lemmon, M. A. & Burger, K. N. J. (2005). Membrane activity of the phospholipase C- $\delta$ 1 pleckstrin homology (PH) domain. *Biochem. J.* **389**, 435-441.
62. Herzog, F. A., Braun, L., Schoen, I. & Vogel, V. (2016). Improved side chain dynamics in MARTINI simulations of protein lipid interfaces. *J. Chem. Theor. Comput.* **12**, 2446-2458.
63. Rameh, L. E., Arvidsson, A. K., Carraway, K. L., Couvillon, A. D., Rathbun, G., Crompton, A., VanRenterghem, B., Czech, M. P., Ravichandran, K. S., Burakoff, S. J., Wang, D. S., Chen, C. S. & Cantley, L. C. (1997). A comparative analysis of the phosphoinositide binding specificity of pleckstrin homology domains. *J. Biol. Chem.* **272**, 22059-22066.
64. Maffucci, T. & Falasca, M. (2001). Specificity in pleckstrin homology (PH) domain membrane targeting: a role for a phosphoinositide-protein co-operative mechanism. *FEBS Lett.* **506**, 173-179.
65. Isakoff, S. J., Cardozo, T., Andreev, J., Li, Z., Ferguson, K. M., Abagyan, R., Lemmon, M. A., Aronheim, A. & Skolnik, E. Y. (1998). Identification and analysis of PH domain-containing targets of phosphatidylinositol 3-kinase using a novel in vivo assay in yeast. *EMBO J.* **17**, 5374-5387.
66. Yamamoto, E., Akimoto, T., Kalli, A. C., Yasuoka, K. & Sansom, M. S. P. (2017). Dynamic interactions between a membrane binding protein and lipids induce fluctuating diffusivity. *Sci. Adv.* **3**, e1601871.
67. Huang, B. X., Akbar, M., Kevala, K. & Kim, H.-Y. (2011). Phosphatidylserine is a critical modulator for Akt activation. *J. Cell Biol.* **192**, 979-992.
68. Lucas, N. & Cho, W. (2011). Phosphatidylserine binding is essential for plasma membrane recruitment and signaling function of 3-phosphoinositide-dependent kinase-1. *J. Biol. Chem.* **286**, 41265-41272.
69. Gallego, O., Betts, M. J., Gvozdenovic-Jeremic, J., Maeda, K., Matetzki, C., Aguilar-Gurrieri, C., Beltran-Alvarez, P., Bonn, S., Fernandez-Tornero, C., Jensen, L. J., Kuhn, M., Trott, J., Rybin, V., Muller, C. W., Bork, P., Kaksonen, M., Russell, R. B. & Gavin, A. C. (2010). A systematic screen for protein-lipid interactions in *Saccharomyces cerevisiae*. *Molec. Systems Biol.* **6**.
70. Vonkova, I., Saliba, A.-E., Deghou, S., Anand, K., Ceschia, S., Doerks, T., Galih, A., Kugler, Karl G., Maeda, K., Rybin, V., van Noort, V., Ellenberg, J., Bork, P. & Gavin, A.-C. (2015). Lipid cooperativity as a general membrane-recruitment principle for PH domains. *Cell Reports* **12**, 1519-1530.

71. Bereau, T., Bennett, W. F. D., Pfaendtner, J., Deserno, M. & Karttunen, M. (2015). Folding and insertion thermodynamics of the transmembrane WALP peptide. *J. Chem. Phys.* **143**.
72. Hess, B., Kutzner, C., van der Spoel, D. & Lindahl, E. (2008). GROMACS 4: algorithms for highly efficient, load-balanced, and scalable molecular simulation. *J. Chem. Theor. Comp.* **4**, 435-447.
73. Monticelli, L., Kandasamy, S. K., Periole, X., Larson, R. G., Tieleman, D. P. & Marrink, S. J. (2008). The MARTINI coarse grained force field: extension to proteins. *J. Chem. Theor. Comp.* **4**, 819-834.
74. Marrink, S. J., Risselada, J., Yefimov, S., Tieleman, D. P. & de Vries, A. H. (2007). The MARTINI force field: coarse grained model for biomolecular simulations. *J. Phys. Chem. B.* **111**, 7812-7824.
75. Hess, B., Bekker, H., Berendsen, H. J. C. & Fraaije, J. G. E. M. (1997). LINCS: A linear constraint solver for molecular simulations. *J. Comp. Chem.* **18**, 1463-1472.
76. Humphrey, W., Dalke, A. & Schulten, K. (1996). VMD - Visual Molecular Dynamics. *J. Molec. Graph.* **14**, 33-38.
77. Eastwood, M. P., Hardin, C., Luthey-Schulten, Z. & Wolynes, P. G. (2001). Evaluating protein structure-prediction schemes using energy landscape theory. *IBM J. Res. Develop.* **45**, 475-497.